JOURNAL OF APPLIED PHYSICS **110**, 034510 (2011)

Analytical drain current model reproducing advanced transport models in nanoscale cylindrical surrounding-gate (SRG) MOSFETs

M. Cheralathan,[1,a)] G. Iannaccone,[2] E. Sangiorgi,[3] and B. Iñiguez[1]
[1]*DEEEA, Universitat Rovira i Virgili (URV), Tarragona 43007, Spain*
[2]*Department of Information Engineering, University of Pisa-IU.NET, Pisa 56122, Italy*
[3]*ARCES, University of Bologna-IU.NET, Cesena 47521, Italy*

(Received 20 May 2011; accepted 13 June 2011; published online 11 August 2011)

In this paper we extend a compact surrounding-gate MOSFET model to include the hydrodynamic transport and quantum mechanical effects, and we show that it can reproduce the results of 3D numerical simulations using advanced transport models. A template device representative for the cylindrical surrounding-gate MOSFET was used to validate the model. The final compact model includes mobility degradation, drain-induced barrier lowering, velocity overshoot, and quantum effects. Comparison between the compact model and the advanced transport modeling approaches shows good agreement within the practical range of drain voltages. © *2011 American Institute of Physics*. [doi:10.1063/1.3618678]

I. INTRODUCTION

The advantages of silicon-on-insulator (SOI) MOSFETs over bulk transistors related to reduced short channel effects, lower parasitic capacitances, and increased circuit speed are well known. Among SOI devices, surrounding-gate (SRG) has become one the most promising device structures according to the technology scaling roadmap.[1] These devices include important features that permit more aggressive channel length scaling than to their conventional bulk counterparts. In this context, it is important to highlight the efforts currently under way in relation to multigate MOSFETs compact modeling[2–5] The continuous scaling in the IC industry makes the reduction in the active silicon area in multigate MOSFETs essential in order to keep the short channel effects (SCE) under control.[6] Therefore, the influence of structural confinement is increasing, which makes the charge distribution in these devices completely different to that found in conventional bulk. Hence, there is a great need for new compact models that accurately describe the physics of these devices.[7]

Our starting point in this work is an analytical expression that models the variation of surface potential as well as the difference of potential at the surface and at the middle of the silicon layer.[8] The expression obtained for the potentials is used to derive an analytical compact model for the drain current of a cylindrical surrounding-gate MOSFETs. This model was derived for doped devices, but it has been demonstrated to be valid in lightly doped devices. We extend the model to include hydrodynamic transport and quantum mechanical effects. As the channel length is reduced 3D effects appear near the source and drain producing the so-called SCE, such as drain-induced barrier lowering (DIBL). The DIBL effect is considered through a threshold voltage correction in the compact model. Using the concept of an inversion layer centroid, we have introduced a correction in the oxide capacitance to improve the accuracy in the strong inversion region.[7] Velocity overshoot is modeled through the hydrodynamic transport[9] which is also included in the model. The model takes into account the mobility degradation[10] due to scattering effects. The final compact model for the drain current includes hydrodynamic transport, mobility degradation, short channel effects such as DIBL, and quantum effects. Comparisons between the compact model and 3D advanced numerical transport models are shown.

II. dc MODEL

A. Expression for potentials

The potentials at the surface, ϕ_s, and in the center, ϕ_o, of the silicon layer are calculated analytically. The surface potential in the subthreshold ϕ_{sBT} regime are calculated analytically using the Lambert function as:[8]

$$\phi_{sBT} = V_{GS} - V_{fb} - \frac{Q_{dep}}{C^*_{ox}} - \phi_t LW\left[\frac{Q_{dep}}{C^*_{ox}\phi_t} e^{\left(\frac{V_{GS}-V_{fb}-\frac{Q_{dep}}{C^*_{ox}}-V_{ch}-2\phi_F}{\phi_t}\right)}\right] \tag{1}$$

and in the above threshold regime as:

$$\phi_{sAT} = V_{GS} - V_{fb} - 2\phi_t LW\left[\frac{1}{2C^*_{ox}\phi_t}\sqrt{\frac{4Q_{dep}\varepsilon_{si}\phi_t}{R}} \times \sqrt{1 - \frac{1}{\alpha} + \frac{1}{\alpha} e^{-\alpha} e^{\left(\frac{V_{GS}-V_{fb}-V_{ch}-2\phi_F}{2\phi_t}\right)}}\right], \tag{2}$$

where V_{GS} is applied to the gate voltage, V_{fb} is the flatband voltage, $Q_{dep} = qN_aR/2$ is the fixed charge density per unit gate area, N_a is the doping concentration, R is the radius of the cylindrical silicon body, $\phi_t = \frac{kT}{q}$ is the thermal voltage, V_{ch} is the quasi-Fermi potential along the channel, $\phi_F = \phi_t \ln(N_a/n_i)$ is the Fermi potential, $\alpha = (\phi_s - \phi_o)/\phi_t$ is the normalized difference of potentials, ε_{si} is the permittivity of

---

[a)] Author to whom correspondence should be addressed. Electronic mail: muthupandian.cheralathan@urv.cat.

silicon, and q is the electric charge. The inversion centroid is a function of the inversion charge. A simple relationship between inversion centroid and inversion charge obtained by fitting numerical simulation results is given by $\frac{1}{z_I} = \frac{1}{a+2bR} + \frac{1}{z_{IO}}\left(\frac{N_I}{N_{IO}(R)}\right)^n$ (Ref. 7) with $a = 0.55\,\text{nm}$, $b = 0.198$, $z_{IO} = 5.1\,\text{nm}$, $n = 0.75$, and $N_{IO}(R) = 8.26 \times 10^{12}\text{cm}^{-2} \; - 4.9 \times 10^{18}\text{cm}^{-3} \times R(\text{cm})$. The classical oxide capacitance C_{ox} was replaced in our model by another capacitance, corrected oxide capacitance (C^*_{ox}), where the capacitance of the oxide was in series with a centroid capacitance, which is the capacitance of a silicon layer, given as:[7]

$$\frac{1}{C^*_{ox}} = \frac{1}{C_{ox}} + \frac{1}{C_{cen}}, \tag{3}$$

where $C_{cen} = \frac{\varepsilon_{si}}{(R-z_I)\ln\left(1+\frac{z_I}{(R-z_I)}\right)}$, and $C_{ox} = \frac{\varepsilon_{ox}}{R\ln\left(1+\frac{t_{ox}}{R}\right)}$ is the oxide capacitance per unit gate area in a SRG MOSFET; t_{ox} is the oxide thickness and ε_{ox} is the permittivity of the oxide.

The final surface potential in all regimes are calculated as:

$$\begin{aligned}\phi_s = {} & \phi_{sBT}\frac{1}{2}\{1 - \tanh[10(V_{GS} - V_T - V_{ch})]\} \\ & + \phi_{sAT}\frac{1}{2}\{1 + \tanh[10(V_{GS} - V_T - V_{ch})]\},\end{aligned} \tag{4}$$

where V_T is the threshold voltage as shown in Ref. 8.

B. Mobile charge

Mobile charge as a function of the surface potential is obtained by solving Poisson's equation. Their normalized values at the source, q_S, and at the drain, q_D, are given by the following expression as in Ref. 8:

$$q_{S(D)} = \sqrt{\frac{4q_{dep}\varepsilon_{si}}{C^*_{ox}R}}\sqrt{\alpha}\sqrt{\frac{1}{2} + \left[\frac{1 - \frac{1}{\alpha} + \frac{1}{\alpha}e^{-\alpha}}{\alpha}\right]e^{\frac{\phi_s - V_{S(D)} - 2\phi_F}{\phi_t}}} - q_{dep}, \tag{5}$$

where $q_{dep} = \frac{Q_{dep}}{C^*_{ox}\phi_t}$ is the normalized fixed charge density per unit gate area.

C. DIBL effect

The drain-induced barrier lowering (DIBL) is considered through a threshold voltage correction ΔV_T as:[11]

$$\Delta V_T = \sigma\phi_F\left(\frac{L_c}{L}\right)^2\left[1 - e^{\left(-\frac{L}{0.25L_m}\right)}\right]\left[1 + \frac{|V_{ch}|}{3.6\phi_t} - e^{\left(\frac{|V_{ch}|}{2.5\phi_t}\right)}\right], \tag{6}$$

where σ is the fitting parameter, L_m is a reference length $= 1 \times 10^{-5}\text{cm}$ and $L_c = \sqrt{\frac{2\varepsilon_{si}R^2\ln\left(1+\frac{2t_{ox}}{R}\right)+\varepsilon_{ox}R^2}{16\varepsilon_{ox}}}$ is the characteristic length.[12]

One of the most used expressions for the saturation potential[13] has been corrected as

$$V_{dssat} = \left(-\frac{Q_{seff}}{C^*_{ox}}\right)\left(\frac{v_{sat}}{\left(\frac{-Q_{seff}\mu_{eff}}{2LC^*_{ox}}\right) + v_{sat}}\right) \tag{7}$$

with

$$Q_{seff} = q_s + 4\frac{kT}{q}C^*_{ox}\left(\frac{v_{sat}}{v_{sat} - \frac{kT}{q}\left(\frac{\mu_{eff}}{L}\right)}\right), \tag{8}$$

where v_{sat} is the saturation velocity.

The effective drain voltage valid in the linear and saturated region is calculated as:

$$\begin{aligned}V_{Def} = {} & V_{dssat} + \frac{1}{2}\left[\left(V_{ch} - V_{dssat} - \frac{\phi_t}{3}\right)\right. \\ & \left. - \sqrt{\left(V_{ch} - V_{dssat} - \frac{\phi_t}{3}\right)^2 + 4\frac{\phi_t}{3}V_{dssat}}\right].\end{aligned} \tag{9}$$

In the subthreshold region, the effective voltage must be adjusted to represent the real behaviors, so a complementary effective drain voltage is defined as:

$$\begin{aligned}V_{Defs} = {} & V_D\frac{1}{2}\{1 - \tanh[5(V_{GS} - V_T)]\} \\ & + V_{Def}\frac{1}{2}\{1 + \tanh[5(V_{GS} - V_T)]\}.\end{aligned} \tag{10}$$

A smoothing function is used to interpolate V_{dss}:

$$V_{dss} = V_{Defs} - \frac{kT}{q}\frac{\ln\{1 + \exp\left[A\left(V_{Defs} - V_{dssat}\right)/(kT/q)\right]\}}{A}, \tag{11}$$

where A is the parameter that controls the transition between saturated and nonsaturated channels

D. Velocity overshoot

In extremely short channel multigate MOSFET the transport regime is quasi-ballistic, thus an important overshoot velocity is expected. Using a simplified energy-balance model, the electron mobility is a function of the electron temperature related to the average energy of the carriers. The electron temperature T_e is governed by the following equation:[9]

$$\frac{dT_e}{dx} + \frac{T_e - T_O}{\lambda_w} = -\frac{q}{2k}E_x(x), \tag{12}$$

where the energy-relaxation length is defined as $\lambda_w \approx 2v_{sat}\tau_w$, τ_w being the energy relaxation time constant, v_{sat} the saturation velocity, and $E_x(x)$ is the lateral electric field.

The velocity increases along the channel, and at the saturation voltage, the velocity reaches a saturation velocity. Assuming that the velocity is saturated we can divide the channel into two sections: the first section $0 < x < L_e = L - L_{sat}$, and the saturation region, $x > L_e$. In contrast with classical drift-diffusion models, the saturated velocity in the saturation region due to nonstationary effects can achieve several times the stationary saturation velocity, v_{sat}. This phenomenon is known as velocity overshoot. The velocity overshoot has been modeled through a hydrodynamic transport model.

E. Drain current

The drain-current in a SRG MOSFET is calculated as a function of the mobile-charge densities at the source Q_s and at the drain Q_d[8]

$$I_{DS} = \frac{W\mu_{eff}}{L_e(1+\gamma_n V_{dss})}\left[2(q_S - q_D) + \frac{q_S^2 - q_D^2}{2} + 2q_{dep}\ln\left[\frac{q_D + 2q_{dep}}{q_S + 2q_{dep}}\right]\right]. \tag{13}$$

The effective mobility is defined as:[10]

$$\mu_{eff} = \frac{\mu_o}{1 + \theta_1\beta\log(1+\exp(1+(V_{GS}-V_T)/\beta) + \theta_2\beta^2\log(1+\exp(1+(V_{GS}-V_T)/\beta)^2}, \tag{14}$$

where μ_o is the low-field mobility, and θ_1 and θ_2 are the mobility attenuation coefficients of the first and second orders, respectively, which can be considered as fitting parameters, $\gamma_n = \frac{\mu_{eff}}{v_{sat}L}(\frac{1}{1+2\lambda_w/L})$; V_{dss} is equal to V_{Defs} for a nonsaturated channel and $V_{dss} = V_{dssat}$ for a saturated channel; $L_e = L - \Delta L$ and $W = 2\pi R$ are the device effective length and width respectively, where the saturated channel length is given by $\Delta L = L_c \arcsin h(\frac{V_{Defs}-V_{dssat}}{E_{sat}L_c})$, and E_{sat} is the saturation field when velocity reaches the saturation velocity.

III. SIMULATED DEVICE AND APPROACHES

We consider the cylindrical SRG MOSFET shown in Fig. 1. It has a physical gate length of 6 nm and a gate stack consisting of 2 nm of HfO2 on top of 0.7 nm of SiO2 [Effective oxide thickness (EOT) = 1 nm]. The channel is lowly doped (10^{15} cm^{-3}). The channel diameter is 4 nm.

Each model is identified with the acronym of the main developer. The possible modeling approaches range from modifications of the conventional drift-diffusion (DD) model used in commercial TCAD tools to advanced Monte Carlo models. The different numerical models used by the different groups[14–17] differ in terms of scattering mechanisms, simulation approaches, and so on. In order to compare, all simulators have been calibrated first to reproduce the curves in silicon devices.

A. SNPS (Synopsis Switzerland LLC)

In the SNPS model,[14] at low drain bias, the effect of mobility degradation is seen at higher gate voltages.

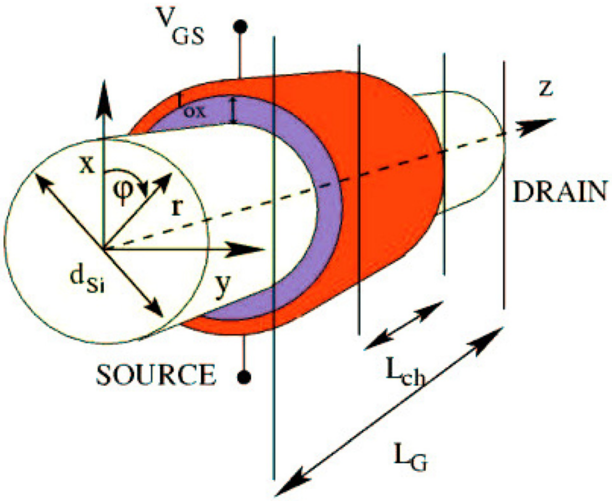

FIG. 1. (Color online) Structure of the cylindrical SRG MOSFET template used in this work.

B. SNPS with ion impurities (II)

In SNPS with ion impurities (II),[14] the drain current has a stronger mobility degradation effect when compared to the other groups. The effect of ion impurity scattering has a strong influence on the drain current and, hence, the drain current is lower than in the other groups.

C. IUNET (Consorzio Nazionale Interuniversitario per la Nanoelettronica)-University of Bologna (quantum ballistic)

The tight-binding approach is employed to work out the system Hamiltonian on quantum transport under ballistic condition.[15] The mobility degradation is not significant. It can be seen that the velocity saturation takes place at higher values.

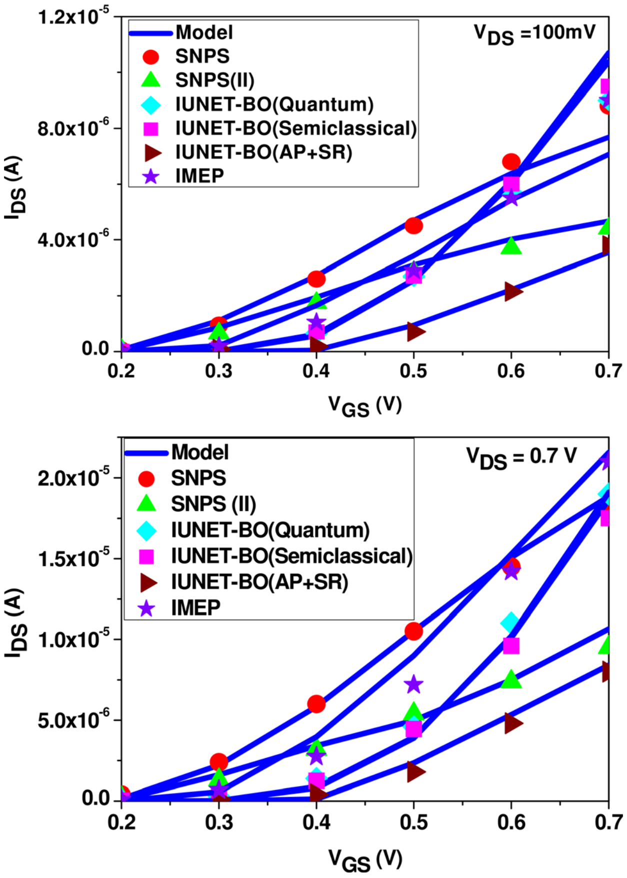

FIG. 2. (Color online) Transfer characteristics of the cylindrical SRG MOSFET (Fig. 1) for low (top) and high (bottom) V_{DS}. 3D numerical simulation data by Synopsys (SNPS; Ref. 14), University of Bologna (IUNET-BO; Refs. 15 and 16), and IMEP (Ref. 17).

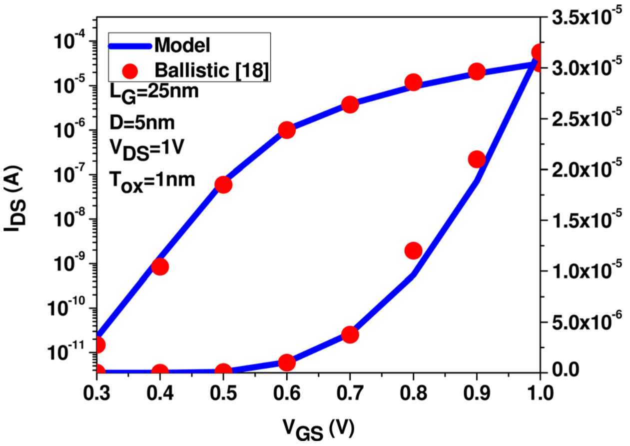

FIG. 3. (Color online) Transfer characteristics of a cylindrical SRG MOSFET at high V_{DS} both in linear and logarithmic scale.

TABLE I. Parameters used in the proposed analytical model in order to fit the simulations obtained from advanced transport models.

	Cylindrical SRG MOSFET $L_G = 6$ nm Dsi = 4 nm EOT = 1.0 nm device parameters		
Models	V_{sat} (cm/sec)	θ_1 (V^{-1})	θ_2 (V^{-2})
SNPS	1.5	3.35	0.7
SNPS (Ion Impurities)	1.65	6.15	1.1
IUNET-BO (Quantum Ballistic)	1.05	0	0
IUNET-BO (Semiclassical Ballistic)	1.05	0	0
IUNET-BO (Acoustic Phonon and Surface Roughness)	1.45	5.25	2.55
IMEP	1.35	3.25	0.55

D. IUNET-BO (semiclassical ballistic)

Scattering events are accounted for via relaxation-time approximation, which holds for elastic collisions only.[16] The mobility degradation is not significant.

E. IUNET-BO (acoustic phonon and surface roughness)

In IUNET-BO with acoustic phonon (AP) and surface roughness (SR),[16] the mobility degradation has a slight influence on the drain current. Also, the effect of velocity saturation is stronger than in the other groups, which can be seen clearly.

F. IMEP (Institut de Microélectronique, Electromagnétisme et Photonique), Grenoble (France)

In IMEP model,[17] the drain current is higher than other models considered in this paper. It considers backscattering. The effect of mobility degradation is lower when compared to other models which consider scattering.

IV. RESULTS AND DISCUSSION

The results of the compact model have been compared with the 3D numerical simulation data obtained by several research groups using advanced transport models[14–17] Figure 2 shows the transfer characteristics of the cylindrical SRG MOSFET at low and high V_{DS}. A good agreement between the compact model and the 3D numerical simulations[14–17] is obtained by considering the low field mobility and for a fitted saturation velocity. In the transfer characteristics it can be clearly noted that the mobility degradation at low drain voltages is significantly reproduced by the compact model. In the IMEP model it can be observed that the effect of the mobility degradation parameter is lower when compared to the other models, which may be due to the fact that surface roughness scattering is not considered in the IMEP model.

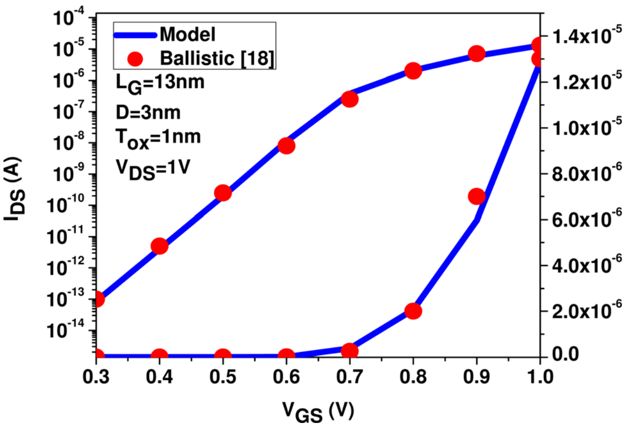

FIG. 4. (Color online) Transfer characteristics of a cylindrical SRG MOSFET at high V_{DS} both in linear and logarithmic scale.

Figure 3 shows the transfer characteristics of a longer channel cylindrical SRG MOSFET at high V_{DS}. A good agreement between the compact model and the 3D numerical simulation data[18] is obtained both in subthreshold and above threshold by considering the low field mobility and for a fitted saturation velocity.

Figure 4 shows the transfer characteristics of an $L_G = 13$ nm cylindrical SRG MOSFET at high V_{DS}. Also, a good agreement between the compact model and the 3D numerical simulation data[18] is obtained both in subthreshold and above threshold by considering the low field mobility and for a fitted saturation velocity.

Table I indicates the mobility degradation and velocity saturation parameter values that have been considered in the model to fit the different numerical simulations of the SRG MOSFET shown in Fig. 1. From the Table 1 parameters it can be seen that a strong mobility degradation is observed with the SNPS (ion impurities) model. It can be seen that a lower mobility degradation is observed with the IMEP model, as discussed before.

TABLE II. Parameters used in the proposed analytical model in order to fit the simulations obtained from advanced transport models.

	Cylindrical SRG MOSFET $L_G = 25$nm Dsi = 5nm			Cylindrical SRG MOSFET $L_G = 13$nm Dsi = 3nm		
Model	V_{sat} (cm/sec)	θ_1 (V^{-1})	θ_2 (V^{-2})	V_{sat} (cm/sec)	θ_1 (V^{-1})	θ_2 (V^{-2})
Ballistic (Ref. 18)	1.05	0	0	1.05	0	0

Table II shows the mobility degradation and velocity saturation parameter values that have been used to fit the numerical simulations of Ref. 18, which is a longer-channel device SRG MOSFET.

V. CONCLUSIONS

We have extended our previous cylindrical SRG MOSFET model to include hydrodynamic transport, short channel effects, mobility degradation due to scattering mechanisms, velocity overshoot, and quantum effects. The comparisons between the advanced numerical transport models and the compact model for the drain current in cylindrical SRG MOSFET show that if our compact model includes the hydrodynamic transport model it can reproduce those simulation results based on 3D advanced transport models. The model is valid and continuous in all regimes.

ACKNOWLEDGMENTS

Work supported by the MICINN (Spanish Government) under project TEC2008-06758-C02-02; by the EU under contracts 216171 “NANOSIL”, 218255-“COMON”, and EU SQWIRE (FP7-ICT-STREP no. 257111); by the ICREA Academia Award and by the PGIR grant (URV). Professor Enrico Sangiorgi acknowledges the grant from Fondazione Cassa dei Risparmi di Forlì.

[1] International Technology Roadmap for Semiconductors; 2009 and the 2010 update. http://public.itrs.net.

[2] D. Jimenez, B. Iniguez, J. Su, L. F. Marsal, J. Pallares, J. Roig, and D. Flores, IEEE Electron Device Lett. **25**(8), 571 (2004).

[3] B. Iniguez, D. Jimenez, J. Roig, H. A. Hamid, L. F. Marsal, and J. Pallares, IEEE Trans. Electron Devices **52**(8), 1868 (2005).

[4] A. Lazaro and B. Iniguez, Semicond. Sci. Technol. **23**(7), 075022 (2008).

[5] J. B. Roldan, A. Godoy, F. Gamiz, and M. Balaguer, IEEE Trans. Electron Devices **55**(1), 411 (2008).

[6] C. P. Auth and J. D. Plummer, IEEE Electron Device Lett. **18**(2), 166 (1997).

[7] J. B. Roldan, F. Gamiz, F. Jimenez-Molinos, C. Sampedro, A. Godoy, F. G. Ruiz, and N. Rodriguez, IEEE Trans. Electron Devices **57**(11), 2925 (2010).

[8] M. Cheralathan, A. Cerdeira, and B. Iñiguez, Solid State Electron. **55**(1), 13 (2011).

[9] A. Lázaro, B. Nae, O. Moldovan, and B. Iñiguez, J. Appl. Phys. **100**, 084320 (2006).

[10] G. Baccarani and S. Reggiani, IEEE Trans. Electron Devices, **46**(8), 1656, (1999).

[11] J. Alvarado, B. Iñigeuz, M. Estrada, D. Flandre, and A. Cerdeira, Int. J. Numer. Model. **23**, 88 (2010).

[12] C. P. Auth, and J. D. Plummer, IEEE Electron Device Lett. **18**(2), 74 (1997).

[13] B. Iñiguez and E. Garcia-Moreno, Analog Integr. Circuits Signal Process. **13**(3), 241 (1997).

[14] “Sentaurus Device Monte Carlo User’s Manual,” Release D-2010.03, pp. 241–244, March 2010.

[15] E. Gnani, S. Reggiani, A. Gnudi, P. Parruccini, R. Colle, M. Rudan, and G. Baccarani, IEEE Trans. Electron Devices **54**(9), 2243 (2007).

[16] E. Gnani, A. Gnudi, S. Reggiani, and G. Baccarani, IEEE Trans. Electron Devices **55**(11), 2918 (2008).

[17] R. Clerc, P. Palestri, L. Selmi, G. Ghibaudo, “Back-Scattering in Quasi Ballistic NanoMOSFETs: The role of non thermal carrier distributions,” paper presented at *Ultimate Integration of Silicon, 2008, 9th International Conference on ULIS* pp. 125–128, 12–14 March 2008.

[18] M. Lenzi, P. Palestri, E. Gnani, S. Reggiani, A. Gnudi, D. Esseni, L. Selmi, and G. Baccarani, IEEE Trans. Electron Devices **55**(8), 2086 (2008).